A method to integrate patterned electrospun fibers with microfluidic systems to generate complex microenvironments for cell culture applications

Patric Wallin,[1] Carl Zandén,[2] Björn Carlberg,[2] Nina Hellström Erkenstam,[3] Johan Liu,[2,a)] and Julie Gold[1,a)]
[1]*Department of Applied Physics, Biological Physics, Chalmers University of Technology, SE-41296 Gothenburg, Sweden*
[2]*Department of Microtechnology and Nanoscience MC2, Bionano Systems, Chalmers University of Technology, SE-41296 Gothenburg, Sweden*
[3]*Center for Brain Repair and Rehabilitation, Institute for Neuroscience and Physiology, University of Gothenburg, SE-41390 Gothenburg, Sweden*

(Received 20 December 2011; accepted 1 June 2012; published online 19 June 2012)

The properties of a cell's microenvironment are one of the main driving forces in cellular fate processes and phenotype expression *in vivo*. The ability to create controlled cell microenvironments *in vitro* becomes increasingly important for studying or controlling phenotype expression in tissue engineering and drug discovery applications. This includes the capability to modify material surface properties within well-defined liquid environments in cell culture systems. One successful approach to mimic extra cellular matrix is with porous electrospun polymer fiber scaffolds, while microfluidic networks have been shown to efficiently generate spatially and temporally defined liquid microenvironments. Here, a method to integrate electrospun fibers with microfluidic networks was developed in order to form complex cell microenvironments with the capability to vary relevant parameters. Spatially defined regions of electrospun fibers of both aligned and random orientation were patterned on glass substrates that were irreversibly bonded to microfluidic networks produced in poly-dimethyl-siloxane. Concentration gradients obtained in the fiber containing channels were characterized experimentally and compared with values obtained by computational fluid dynamic simulations. Velocity and shear stress profiles, as well as vortex formation, were calculated to evaluate the influence of fiber pads on fluidic properties. The suitability of the system to support cell attachment and growth was demonstrated with a fibroblast cell line. The potential of the platform was further verified by a functional investigation of neural stem cell alignment in response to orientation of electrospun fibers versus a microfluidic generated chemoattractant gradient of stromal cell-derived factor 1 alpha. The described method is a competitive strategy to create complex microenvironments *in vitro* that allow detailed studies on the interplay of topography, substrate surface properties, and soluble microenvironment on cellular fate processes. [http://dx.doi.org/10.1063/1.4729747]

INTRODUCTION

Cell microenvironments play a key role in determining cellular fate processes and phenotype expression. Consequently, it is of importance to be able to generate cell microenvironments *in vitro* that can be tightly controlled in order to mimic *in vivo* conditions, induce a

[a)]Authors to whom correspondence should be addressed. Electronic mail: johan.liu@chalmers.se and julie.gold@chalmers.se.

desired cell behavior, or for basic studies on the relative role of specific environmental cues in such processes. Cell microenvironments in two- and three-dimensional culture are defined by several basic parameters: substrate topography, surface chemistry, substrate stiffness and mechanical deformation, shear stress, cell culture media composition, and physiochemical conditions (temperature, *p*H, O_2, CO_2).[1] The ability to manipulate all or some of these parameters is of high importance in many cell biology and biotechnology areas. For example, in tissue engineering and regenerative medicine, one controls microenvironments in order to create a well-defined stem cell niche *in vitro*.[2–7] *In vivo* many different stem cell niche microenvironments exist, which control cell self-renewal and differentiation in various situations. Therefore, there is a large interest to design systems able to mimic such conditions *in vitro*. However, the importance of defined microenvironments is not limited to stem cells, but extends to cancer research,[8–11] drug screening,[12,13] and immunological studies,[14,15] among others. *In vitro* organ models have been generated to achieve these aims, and approaches are even undertaken to combine organ-models in order to create an *in vitro* mimic of the body using microfluidic and lab-on-a-chip techniques.[16]

Spatial and temporal gradients in *in vitro* model systems cannot be easily generated using standard cell culture principles, whereas microfluidic networks are much better suited for this application.[1,17] Microfluidic chips allow the delivery of a variety of signaling molecules to the cells in a highly controlled manner.[18–20] Due to the small dimensions of microfluidic channels, the viscous forces are typically much larger than the inertial forces and this is expressed in a low Reynolds number. As a result, the flow profile in microfluidic channels is laminar and mixing of two parallel fluid streams is limited to diffusion at the interface between the streams.[21] Microfluidic channels thus offer a very well-suited technology to control soluble cues in a microenvironment around cells, for example, through formation of stable liquid gradients,[20] fast switching of liquids,[22] and temporal increase in concentration of certain substances.[23] Chemical gradients of soluble cell-signaling molecules, such as growth factors, cytokines, and chemokines, are of particular interest since they play an important role in most *in vivo* processes, including cell migration and cell differentiation.[24–26] Furthermore, concentration gradients of test compounds in cell media are useful for studies to evaluate cellular responses over a wide range of concentrations in drug discovery.[27] In general, microfluidic gradient generators can be divided into flow-based and free-diffusion-based systems.[20] In this study, a flow-based gradient generator was used which is based on a design original developed by Jeon *et al.*[28] It relies on repetitive splitting and recombining fluid streams with different concentrations. This principle allows the formation of linear and parabolic gradients with varying gradient steepness and profiles,[29] as well as dynamic manipulation of the gradient, by controlling the flow rate in each individual inlet over time.[30]

Besides being able to tightly control the soluble microenvironment, it is known that the surface topography of the cell growth substrate has significant effects on cell signaling and behavior.[4] Electrospinning is a fabrication technique that has received increasing attention during the last few decades as a simple and useful route to obtain macroscopically long polymer fibers of micro- and nanoscale diameter which have a wide range of potential applications.[31,32] Within the biomedical area, electrospun fibers have emerged as promising candidates and useful substrates for cell growth both for *in vivo* and *in vitro* applications.[33–35] The attractive potential of electrospinning is mainly due to the possibility to structurally mimic fibrous components found in the extra-cellular matrix of biological tissue and is therefore being exploited to fabricate scaffolds in the field of tissue engineering.[31,36] One fundamental challenge limiting their use, however, is that the inherently small pore size of electrospun fiber mats is restrictive to cell permeation. The problem is a direct consequence of the small fiber diameters resulting in a densely stacked architecture during the deposition and remains a major challenge in the design and fabrication of electrospun scaffolds.[37] Several different techniques that can facilitate larger pore size and cellular invasion into the fibrous meshes have been proposed, such as combining microfibers with electrospun nanofibers[38] or the use of a gel as a second phase between.[39] However, in parallel to these efforts, extensive attention is still directed towards understanding the influence of physical, chemical and topographical features of various electrospun fibers on cell

attachment,[40,41] morphology,[42] proliferation,[43] differentiation,[44,45] and migration.[46,47] Thin fiber mats, being on average one to a few fiber layers thick, form more of a two-dimensional surface that provides the same chemical and topographical features of individual fibers and their orientation as in three-dimensional matrices, but at the same time allows the traditional investigation of cell attachment, spreading and migration on flat substrates.

In order to explore the full potential of electrospun fiber substrates and investigate cellular responses in greater detail in highly controlled liquid microenvironments, we believe it is beneficial and very interesting to combine fibers with microfluidic channels. This combination enables tight control over soluble cues and surface topology, two important parameters of the cellular microenvironment. We have recently shown the ability to spatially pattern random, as well as directionally oriented, electrospun fiber pads on a single glass substrate by direct photolithographic processing and this forms the underlying foundation for the method described in this study.[48] The combination of aligned electrospun fibers of varying orientation with a microfluidic generated gradient has a large potential to closely mimic certain *in vivo* conditions with one particular example being axon outgrowth. It is known that axon outgrowth in the developing central nervous system is guided and controlled by various chemical and physical cues. Neurotrophins, including nerve growth factor and brain-derived neurotrophic factor among others, are important chemical regulators in the developing brain. Furthermore, stromal cell-derived factor 1 alpha (SDF-1a), a small cytokine, promotes neural stem cell migration to pathological sites in the brain for regeneration.[49] Spatial, as well as temporal, gradients of these molecules have a large effect on axon outgrowth and cell migration. It has also been known for many decades that axonal outgrowth and cell migration are influenced by physical features such as extra-cellular matrix (ECM) stiffness and contact guidance cues.[50] A better understanding of these complex processes is essential to develop new medical therapies for neurodegenerative diseases, stroke and brain trauma, to overcome the limited self-repair capacity of the brain. Both chemical[49] and physical cues[50] have been studied in *in vitro* model system, but to the best of our knowledge only separately.

In this study, we developed and evaluated a method to integrate electrospun fibers with microfluidic networks. The electrospun fiber mats present a surface topology to the cells that can be changed in respect to fiber morphology, fiber patterns, and orientation. This surface topology mimics the conditions found *in vivo*, where radial glial cells are spanning long distances inside the developing brain and act as contact guidance for neural stem cells.[51] Whereas the microfluidic network allows the formation of chemical gradients to mimic neurotrophic gradients found *in vivo*. The ability to combine both techniques and to change the fiber orientation in relation to the applied gradient allows a completely new set of experiments in the future. This includes experiments looking at the interdependency of topographical and chemical cues and investigation on the strength of both cues when they are acting in the same direction or in different directions. The usefulness is further improved by the ability to have multiple fiber alignments in a single chip, allowing quick read out and multi-parametric studies. It is important to point out that the method developed here is not limited to the described system but is applicable in numerous instances where complex biomimetic microenvironments are needed. Additionally, the integration of generic electrospun fiber patterns in this manner does not pose any limitations on the microfluidic design and functionality.

METHODS AND MATERIALS

Electrospinning

A polymer solution was formed by dissolving specific amounts of a biocompatible[43] aromatic polyether based thermoplastic polyurethane (PU) (Desmopan 9370 A, Bayer MaterialScience AG, Germany) in a solvent mixture of tetrahydrofuran (THF) and N,N-dimethylformamide (DMF) (60:40 by weight). To enable photoinitiated covalent cross-linking of the polyurethane resin, 5 wt. % in relation to polymer content of benzoin methyl ether (BME), with a strong absorption in the deep ultraviolet (DUV) region, was added to the polymer solution.[48] Homogenized solutions were transferred to syringes fitted with 19 gauge stainless steel cannuli and electrospun. Random fibers were fabricated in a commercial electrospinning setup (KATO TECH, Japan). The device

was equipped with a slowly rotating conveyor belt, on which glass substrates were attached and subsequently coated with electrospun fibers. Fabrication of aligned fibers was carried out in a custom built setup utilizing parallel grounded electrodes for alignment. During electrospinning, solution was feed at 2 ml/h, while the distance and voltage between the tip of the cannula and the collector plates were kept at 18 cm and 18 kV, respectively.

Direct photolithography of electrospun fibers

A standard mask aligner (KS MJB3, SUSS MicroTec AG, Germany) with a DUV light source (248 nm wavelength) was used for photolithographic patterning. Upon DUV irradiation, utilizing a quartz mask, the BME molecules are subject to an alpha cleavage and free radical formation inducing crosslinking between rigid macromolecular blocks of the segmented polyurethane chains, resulting in significant reduction in the solubility of the exposed regions. Exposure was carried out for 5 min at an intensity of 1.5 mW cm^{-2} (total dose 450 mJ cm^{-2}). As the network is immersed in THF, the unexposed areas will dissolve leaving only the intended patterns on the substrate. Patterns were developed by immersion in THF for 1 min, followed by rinsing in de-ionized water.

Samples with alternating fiber orientation were produced in a double-step process. A first layer of aligned fibers was electrospun utilizing a parallel electrode setup. This layer was spun directly onto a 24×50 mm glass slide that also acted as the carrier substrate for the full device. An array of $250 \times 200\ \mu$m rectangular pads with an $800\ \mu$m pitch was defined by the photolithographic method described above, followed by development in THF and rinsing in de-ionized (DI) water. Subsequently utilizing the same substrate and electrospinning solution and parallel plate setup, a second layer of aligned fibers with perpendicular direction in reference to the first layer was deposited. Finally, in a photolithographic exposure, an interstitial array of rectangular pads was defined with respect to the original pattern, which, after development, resulted in an overall structure of $250 \times 200\ \mu$m pads of $400\ \mu$m pitch with alternating fiber orientation as shown in Figure 2(a)/2(b).

Standard SEM inspection was used to characterize the samples of electrospun fibers, as well as cross-sections of the final microfluidic system. To reduce charging effects, samples were sputter coated with approximately 5 nm gold.

Design and fabrication of microfluidic channels

Microfluidic channels were fabricated in poly-dimethyl-siloxane (PDMS) by standard soft lithography methods described previously.[52] In brief, microfluidic networks were designed in AutoCAD 2010 (Autodesk, USA) and files were used to produce a chrome photomask using electron beam lithography (JEOL JBX-5DII, Japan). The mask was utilized to photo pattern 50 micrometer thick spin coated SU-8 (SU-8 50, MicroChem Co., USA) on silicon wafers via standard photolithography. The resulting device master was used repeatedly for PDMS molding. PDMS pre-polymer (Sylgard 184, Dow Corning Co., USA) was mixed in a 10:1 ratio with curing agent, casted on the device master and cured for 2 h at 95 °C. After curing the PDMS was cut and peeled off from the master. A biopsy punch with an inner diameter of 1.2 mm was used to punch holes through the PDMS for the inlet and outlet ports. The resulting microfluidic channels were $400\ \mu$m wide in the probing channel and $50\ \mu$m wide in the serpentine channel of the gradient generator. The height of the channels was $50\ \mu$m throughout the whole network.

Computational fluid dynamic (CFD) simulations

During the design process CFD simulations in COMSOL (Comsol 4.0 a, Sweden), based on Navier-Stokes equations for incompressible flow, were used to evaluate the different designs and optimize the performance of the gradient network. The gradient network was represented either as a two dimensional model in x-y direction or a three dimensional model. For the final design, a range of suitable flow velocities that produce gradients with a large steep linear region in the center of the channel were assessed by CFD simulation. The diffusion coefficient of

sodium fluorescein was approximated as 5×10^{-6} cm^2/s, in order to be comparable with the experimental data and to verify the simulated model system.[53]

The second model was used to investigate the effects of the fiber pad on the flow properties in more detail. A two-dimensional model approach in the x-z direction was used, limited to a cross-section of the channel with the fiber pad along the axis of flow. The fiber pad was modeled as a porous matrix using the Brinkman equation.[54] The Brinkman equation is a generalization of Darcy's law that allows the modeling of the interface between porous media flow and Navier-Stokes driven free media flow. An effective viscosity parameter μ_e in the equation allows matching of the shear stress boundary condition at the interface between the fiber pad (porous media flow) and the remaining channel (free laminar flow). The porosity of the fiber pad was approximated with mercury porosimetry[55] data and SEM image analysis,[56] and obtained values of porosity were estimated to $\varepsilon_p = 0.7$.

Bonding of microfluidic channels and liquid handling

Glass slides with patterned electrospun fibers were carefully washed around the fibers with a cloth soaked in isopropyl alcohol and extensively rinsed with milliQ water. Both the glass slide and the PDMS microfluidic channel were activated by reactive air plasma (PDC-32 G 18 W Harrick Plasma, USA) for 30 s. The PDMS channel was aligned manually under a stereomicroscope in such a way that the electrospun fiber pad was placed in the center of the probing channel. The irreversibly bonded microfluidic chip was placed in the oven at 95 °C for 20 min to increase the bonding strength further, after which, short silicone tubes (228-0702 VWR Silicone tubing 1.5×3 mm, Belgium) were glued (Elastosil A07, Wacker Silicones AG, Germany) on the inlet and outlet ports. They were later used to connect the microfluidic chip to the pump system.

The pump setup used was designed to maximize the control of fluid handling and was assembled in our lab. Individual pumps (milliGAT LF, GlobalFIA, USA) were used to control the flow rate for each inlet. The pumps allow flow rates down to 0.5 nl/s and were controlled by a LabVIEW (National Instruments, USA) program developed in-house. All fluid connections were made by Teflon tubing (1/16 in. $\times$ 0.18 mm, Genetec AB, Sweden).

Gradient generation and evaluation

Gradients of fluorescent molecules in solution were generated to evaluate the gradient generator and to examine effects of the electrospun fiber pads on the flow behavior of liquid in the channel. In order to evaluate the gradient, intensity line profiles were taken at two positions, position 1 upstream directly at the beginning and position 2 downstream at the end of the fiber pad area. The flow rate was varied between 0.5 nl/s and 500 nl/s to investigate the dependency of the gradient formation on the flow velocity at these two positions. Sodium fluorescein (46960, Sigma-Aldrich, USA) and phosphate buffered saline (PBS) buffer solution were used to form soluble gradients. The standard configuration to produce linear gradients was to have a 10 mM sodium fluorescein PBS solution in inlet 1, 5 mM sodium fluorescein PBS solution in inlet 2 and pure PBS in inlet 3. The gradient was imaged with an upright fluorescence microscope (Axioplan 2, Carl-Zeiss AG, Germany) equipped with a b/w digital camera module (AxioCam, Carl-Zeiss AG, Germany). IMAGEJ (1.43 m, NIH, USA) was used to measure intensity line profiles at positions 1 and 2.

Fibroblasts cell experiments

NIH 3T3 fibroblast cells (93061524, ECACC, UK) were cultured in Dulbecco's Modified Eagle's medium (DMEM, D6546, Sigma-Aldrich, USA) with 10% fetal bovine serum (FBS, A15-105, PAA Laboratories, Austria), 1% L-glutamine (G7513-100 ml, Sigma-Aldrich, USA) and 1% penicillin/streptomycin (P4333-100 ml, Sigma-Aldrich, USA). The bonded microfluidic channel was sterilized with 70% ethanol for 15 min and washed extensively with DMEM prior to cell culture. Cells were introduced to the channel at a concentration of 1 million cells per ml from the outlet by suction at the inlet ports. The cell seeding was monitored under the

microscope and the flow was stopped once the cells were observed in the probing channel. Afterwards, the channel was placed in an incubator (CB150, Binder GmbH, Germany) with 5% CO_2 at 37 °C. The cells were allowed to attach for 2 h without any flow. Subsequently, media flow from the inlets was re-established at a flow rate of 10 nl/s for each inlet, resulting in an average flow velocity of 1.5 mm/s in the probing channel.

After 24 h, the channel was flushed with PBS and cells were fixed with 4% formaldehyde (FO0013005P, Scharlab, Spain) for 30 min at 4 °C under static conditions. The channel was washed again with PBS and cells were stained with a solution of 4′,6-diamidino-2-phenylindole (DAPI 1:500, D8417, Sigma-Aldrich, USA), Alexa Fluor 555 phalloidin (1:200, A34055, Invitrogen Ltd, UK) and 0.1% Triton-X 100 (T8787, Sigma-Aldrich, USA) in PBS for 30 min under static conditions in the dark. The sample was washed extensively with PBS before imaging it with an upright fluorescence microscope (Axioplan 2, Carl-Zeiss AG, Germany).

Neurosphere cell experiments

Wistar rats of both sexes were sacrificed on postnatal day 10 (P10) via inhalation of isofluorane, followed by decapitation (ethical permission obtained from the Swedish Animal Welfare Agency, application number 26/08). Brains were rapidly removed, and the subventricular zones and hippocampi were microdissected into ice-cold PBS with glucose (1 g/l; Invitrogen, USA). Tissue pieces from three animals were combined and processed, starting with fine mincing using a scalpel blade, followed by incubation for 10 min at 37 °C in 0.01% papain (Worthington, Lakewood, NJ, USA)/0.1% Dispase II (Sigma-Aldrich, USA)/0.01% DNaseI (Worthington, Lakewood, NJ, USA)/12.4 mM MgSO4 in HBSS w/o Ca^{2+} and Mg^{2+}. Tissue pieces were gently triturated ten times with a 1 ml pipette, incubated for another 10 min at 37 °C, and the trituration step repeated until an opaque cell suspension was achieved (approximately 10–20 times trituration with a 1 ml pipette). The cell suspension was mixed with 5 ml Neurobasal A medium (NBM; Gibco/Invitrogen, USA) supplemented with B27 (1:50)/glutamax (2 mM)/penicillin-streptomycin (PEST; 100 U penicillin, 100 μg streptomycin) (all from Invitrogen Ltd, UK) and centrifugated at 500 g during 5 min. After centrifugation, supernatant was removed, and cells were resuspended in fresh medium. Viable cells were counted by trypan blue exclusion using a hemacytometer. Cells were seeded at 60 000 cells/ml in non-adhesive cell culture plastic flasks. The medium was supplemented with EGF (20 ng/ml, Invitrogen, Stockholm, Sweden), bFGF (10 ng/ml, PeproTech, UK), and heparin (2 μg/ml, Sigma-Aldrich, USA) every other day. For passaging, cells were collected by centrifugation ($500 \times$ g, 5 min), and the pellet was resuspended in 500 μl Accutase (Sigma-Aldrich, USA), followed by incubation at 37 °C for 2×3 min with intermittent gentle trituration. After enzymatic digestion, neurospheres were triturated first with a 1000-μl pipette followed by a 100-μl pipette, suspended in fresh media, and centrifuged as above.

All substrates for neural stem cell experiments were coated with 50 μg/ml poly-L-ornithine (PORN, P4957, Sigma-Aldrich, USA) in milliQ water for 1 h at room temperature and subsequently with 5 μg/ml laminin (L2020, Sigma-Aldrich, USA) in PBS for 3 h at 37°. Neurospheres were disassociated into single cell solution, as described above, for microfluidic experiments. A single cell solution of neural stem cells was introduced into the microfluidic channels via the outlet port by suction, similar to the way 3T3 cells were seeded. Cells were allowed to attach for 2 h under flow free conditions. After 2 h, the flow was initiated at a flow rate of 10 nl/s for each inlet. The SDF-1a gradient was formed by having cell culture media with 100 ng/ml SDF-1a (S190, Sigma-Aldrich, USA) in inlet 1, 50 ng/ml SDF-1a in inlet 2 (center), and no SDF-1a supplement in inlet 3, producing a linear gradient from 100 ng/ml to 0 ng/ml SDF-1a in cell culture media. Cells were cultured under constant flow for 24 h, before they were fixated and stained, similar to 3T3 cells.

RESULTS AND DISCUSSION

The aim of this work was to develop and evaluate a method for achieving precisely controlled microenvironments by designing a system that integrates the advantages of electrospun fiber structures to define topography, mimicking ECM properties, with microfluidic techniques

to control soluble cues. The method was characterized for a specific implementation of a microfluidic gradient generator combined with different patterns of electrospun fiber pads. Furthermore, the possibility to grow cells in such a system was demonstrated. In contrast to systems shown previously,[57–59] our approach allows straight forward incorporation of topographical features in the micro- and submicrometer range without any limitations on the microfluidic design.

Defining fiber patterns and topography

The overall strategy to integrate and spatially define fibrous topography into microfluidic channels, developed in this study, is based upon a patterning technique, which relies on direct photolithographic definition of patterns in a manner similar to a standard negative resist photolithography process.[48] To construct complex geometries and hierarchical microstructures on a single substrate, the process of deposition and exposure can be repeated multiple times. An illustration of the process steps involved in this specific implementation of the direct photolithographic patterning process for the combination with microfluidic networks is given in Figure 1. The advantage of the developed method is that arbitrary fiber patterns can be combined with user-defined microfluidic networks and both can be tailor-made and adjusted for different experiments. To show the potential, three different fiber patterns were combined with a gradient generating microfluidic network.

The first pattern is composed of $250 \times 200\,\mu$m rectangular pads of aligned fibers with alternating perpendicular orientation. The definition of alternating fiber topographies, as shown in Figure 2(a)/2(b), was achieved by adding one extra round of depositing, exposing, development, and drying (steps 1–4 in Figure 1). As the photolithographic method does not influence previously deposited fiber layers, the possibility to add sequential patterning steps allows for the design and generation of highly complex patterns. The particular implementation of aligned fibers of different orientations is chosen as an example, as it is believed to be of potential relevance, for instance, in the fields of cell locomotion and cell spreading, as touched on in the introduction. Each of the fiber pads can be used as an individual probing area and the effect of different alignments, as well as random fiber orientation, can be studied simultaneously in one single device. The second pattern had similar pads ($250 \times 200\,\mu$m with $400\,\mu$m pitch) but only randomly oriented fibers. The third pattern was a single, continuous, rectangular pad of dimensions $250 \times 4000\,\mu$m not shown. The thickness of each fiber pad was approximately $5\,\mu$m.

To further show the versatility and scalability of the patterning process, additional patterns of fiber pads were fabricated.[60] The patterns essentially illustrate a simple example of the

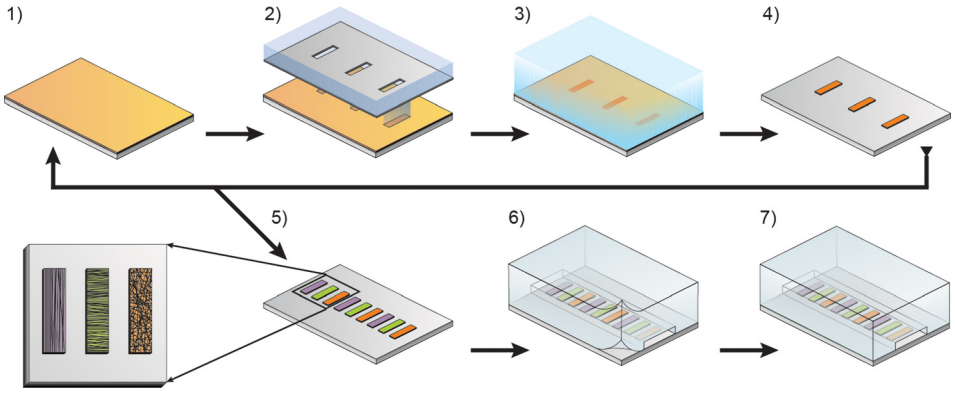

FIG. 1. Process steps for integration of spatially and geometrically defined electrospun fibers into PDMS based microfluidic channels. (1) Polyurethane solution containing BME is electrospun directly onto a glass substrate; (2) the electrospun network is exposed to DUV through a quartz mask causing the BME to form radicals which results in crosslinking of the fiber network; (3) development of the patterns by immersion in THF, dissolving the noncrosslinked areas, followed by rinsing in de-ionized water; (4) substrate is dried and the first layer is complete (5) Process steps 1–4 are repeated consecutively to form new additional fiber pads having different geometries, alignment or fiber diameter; (6) PDMS is molded, aligned and cured onto the glass substrate to form the microfluidic channel around the electrospun patterns; (7) complete microfluidic channel comprising electrospun fibers.

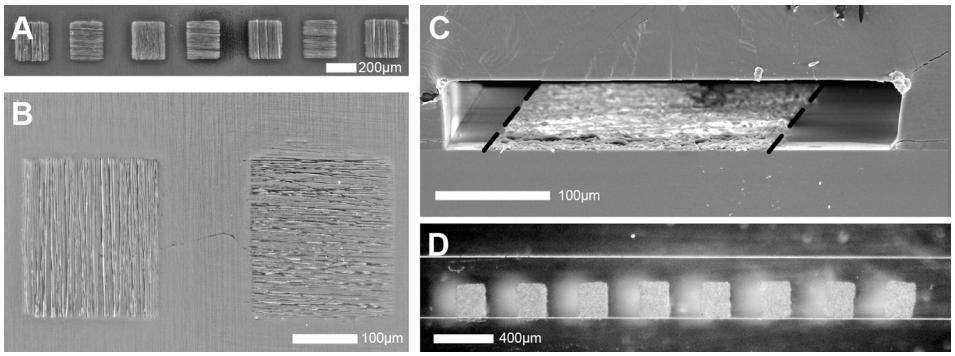

FIG. 2. (a) Scanning electron micrograph of electrospun fiber pads with alternating fiber orientation (alternating vertical and horizontal). The fiber pads are $250 \times 200\ \mu$m with pitch of $400\ \mu$m (center to center distance). (b) Magnified view of (a) showing a fiber pad with vertical fiber orientation to the left and one with horizontal orientation to the right. (c) Scanning electron micrograph of a vertical cross section of the probing channel. The long fiber pad is positioned within the channel, the pad boundaries are indicated by a dashed black line. The PDMS (top) and glass (bottom) are irreversibly bonded and the fiber pad does not disturb the bond. (d) Light micrograph (top view) of electrospun fiber pads within the microfluidic chip. The fiber pads are positioned along the probing channel.

potential and the ability to freely define pattern size and shape using photolithography. They also demonstrate that it is possible to place arrays of fiber sites on the same substrate in order to form multiple microfluidic channels on a single chip or substrate.

In perspective of the presented methodology and results on fabrication of spatially controlled surface morphologies based on photolithographically defined electrospun fibers, it is worthwhile to view and relate this to other approaches aiming at constructing distinct surface morphologies utilizing electrospun fibers or other microfabrication techniques. The method utilized in the present study is characterized by the high spatial resolution capability, repeatability, and quick parallel production. Nevertheless, in contrast to this top-down parallel approach, a number of innovative, bottom-up, serial approaches characterized by controlled deposition of single, continuous, electrospun fibers on a substrate, have emerged.[61] Controlled fiber deposition is typically achieved by reducing the distance to the collector to a point below that of the occurrence of bending instabilities, thus leading to controlled deposition through a straight fiber path.[62–65] For instance, in one implementation of these methods, referred to as direct writing, Brown and co-workers utilized melt electrospinning of poly(ϵ-caprolactone) to fabricate hierarchical electrospun structures by means of a translating collector stage to control fiber localization on a substrate.[61] In this manner, surface morphologies of various geometrical arrangements were achieved, including novel three-dimensional scaffold structures based on fiber stacking. Another prominent example, using novel methodology outside conventional solid-state microfabrication techniques, was presented by Yeong *et al.* in a system utilizing direct femtosecond laser writing on poly(L-lactide-co-ϵ-caprolactone) substrates as a facile route to create micromachined channels for examination of C2C12 myoblast cell alignment and attachment.[66] The channel structure did not only provide cell guidance, but the laser irradiated surfaces also exhibited a microscale roughness promoting cell adhesion towards the substrate indicating suitability of the technology in implant applications. Yet another example include the work by Chang *et al.*, which by novel direct cell microscale freeform fabrication techniques produced three-dimensional *in vivo* like hydrogel-liver cell tissue constructs on substrates, which in turn were integrated in a microfluidic platform.[67] In this manner, a system which provides a biomimetic hydrogel tissue construct for cell culturing in combination with dynamic perfusion and flow shear forces offered by a microfluidic system was achieved. Clearly, a number of methods have been presented so far, each offering individual benefits and drawbacks, and the methodology applied here may act as an alternative or complementary route to acquiring or enhancing functionality in the studies of biologically active microfabricated surface structures, in particular when integrated in a microfluidic platform and exploiting the associated benefits discussed in the introductory section.

An interesting aspect that remains in the scope of further developments, for the system described in this study, is the extension of patterned electrospun fiber topographies into three-dimensional constructs to higher aspect ratios. Essentially this challenge involves the key issue of achieving large porous structures in combination with small fiber diameters to allow sufficient cell penetration into the electrospun networks. The recent trend in scaffold design to overcome this has been to add spacing components that effectively increase the overall pore size of the scaffolds. For instance, Ekaputra *et al*. incorporated biodegradable hyaluronic acid hydrogel into electrospun microfibers through simultaneous electrospraying and showed that this approach allowed for significant improvements in cell infiltration.[39] The approach was also claimed to be beneficial as it potentially allows controlled release of growth factors by utilizing the hydrogel as a release vehicle. In another approach, Pham *et al*. demonstrated a multilayered combination of micro- and nanofibers to generate scaffolds that exploited the resulting large pores from using microfibers to permit cell vertical penetration in combination with the physical mimicry of ECM through the nanofibers.[38] Balancing the ratio of fibers in a multilayered manner undoubtedly has remarkable potential to facilitate the broad needs of electrospun 3D structures. From a perspective of integration with microfluidics only the latter of the two strategies to improve cell infiltration can be expected to be compatible with the process of direct photolithography used in the present study. Additionally, any potential advantages of controlled release of bioactive factor are lessened through the addition of microfluidics to define the chemical microenvironment. Another method, seemingly suitable in combination within a microfluidic based system, was demonstrated by Nandan *et al*. who employed dynamic culture conditions in order to substantially increase cellular ingrowth into a electrospun poly(ε-caprolactone) (PCL) scaffold with fibers of diameters ranging from 300 nm up to 1 μm.[68] Yet an additional way to tackle the problem could be to utilize the direct photolithographic patterning technique to sequentially build up layer by layer of a scaffold. In principle, such an approach could allow for well-defined three dimensional architectures of pore sizes, which are in essence defined through photolithography.

Bonding of microfluidic channels over patterned fibers

PDMS is a commonly used material to produce microfluidic networks by soft lithography due to relatively low costs, high flexibility, and reliability. PDMS has certain advantages for cell culture applications: it is non-cytotoxic, inert to most chemicals, autoclavable, gas permeable and transparent, allowing fluorescence microscopy. On the other hand, it has certain limitations, such as rapid adsorption of small molecules and monomer leakage.[69] A further limitation is that PDMS can only form tight irreversible seals on a very limited number of materials. The bonding efficiency of PDMS and PU electrospun fibers was evaluated with glass slides covered completely with fibers (data not shown). The inability to bond the PDMS directly to the fibers is due to the chemical composition of the PU fibers and the rough surface topology.[70]

The fiber patterning process is thus not only considered useful for forming multiple topographies, but also found to be a key enabling strategy for integration by defining fibers to reside only in areas where they do not restrict the bonding process of the PDMS microchannels. Hence, a tight seal is formed directly between the PDMS and glass substrate with a patterned fiber pad in the center of the channel. The bonding of the PDMS microfluidic network to the glass substrate with the patterned electrospun fiber pads was shown to be successful. It was evaluated by SEM imaging of channel cross-sections, Figure 2(c). The images show clearly that patterned fibers in the channel do not interfere with the glass (bottom) to PDMS (top) bond. Figure 2(d) shows the alignment of a microfluidic channel over patterned electrospun fiber pads.

To the best of our knowledge, only a few examples of combining electrospun fibers and microfluidic system exist in literature. The examples include HIV detection,[71] histidine-tagged protein purification,[72] and cross-array protein immunoassays[73] and are aimed for biosensing applications. However, none of these approaches offer any precise spatial or hierarchical control of the deposition of electrospun fibers, nor the possibility to vary crucial fiber parameters such

as alignment orientation and diameter in the same device. In those studies, large electrospun fiber mats were used and channels were sealed by press fitting. Press fitting can generate tight seals, but the hydraulic pressure that can be applied in such a system is lower compared with irreversible bonded PDMS microfluidic networks. Furthermore, if electrospun fiber pads are located both inside the channel and at the PDMS glass interface,[60] they will allow for a small amount of liquid to slowly creep over the channel boundaries. This effect could be problematic for long term cell culture experiments that run over several days or weeks, due to accumulation of molecules and potential infectious agents in small voids, or in the worst case, complete failure of the seal. Therefore, it is of high relevance to pattern electrospun PU fibers and position the fiber pads within the microfluidic channel in order to obtain an irreversible seal between the glass and the PDMS that is not disrupted by the fibers.

Molecular gradient generation with and without fibers

The effect of cell signaling molecules on cell phenotype expression can be highly dependent on the dose or concentration of the molecule and the context in which it is given. Gradients in concentration of specific substances added to the cell culture media are necessary to examine or more efficiently screen the effect of the substance on cells. Concentration gradient formation in microfluidic channels was studied by CFD simulations, as well as by experiments. Figure 3(a) shows the simulated gradient network and the color coded concentration gradient (red = 100%, blue = 0%) in the probing channel at different flow rates. On the left side, it can be seen how liquid of different concentrations (0, 50, and 100%) from the three inlets is split and recombined to eventually result in nine separate channels that are joined in the probing channel, forming the concentration gradient. The right part of Figure 3(a) shows the influence of three different flow rates on the gradient properties. For an average velocity of 15 mm/s, the gradient is well established throughout the whole channel (top image), while for 1.5 mm/s, the gradient looks similar at the beginning of the channel but is less steep at the end of the probing channel (middle image) compared with higher velocities. Since mixing in microfluidic channels is governed by diffusion, the gradient will be sharper at the beginning of the probing channel than at the end and steeper for high flow velocities compared to low flow velocities. The effect of diffusion is even more pronounced for 0.075 mm/s (lower image), where the gradient is not well established and is nearly vanished at the end of the channel. It can be seen that diffusion is even reducing the gradient steepness at the first measurement position, because this position is 2 mm downstream from the point where the 9 inlets from the gradient generator are recombined.

For the experimental evaluation of the gradient, a concentration gradient of sodium fluorescein was formed under different flow rates, and images of fluorescein solution in the channel were taken with a fluorescence microscope. Figure 3(b) shows a bright field image of the second measurement position at the downstream end of the fiber pads, whereas Figure 3(c) shows the corresponding fluorescence image at the same position. This image (Figure 3(c)) shows a clear gradient in fluorescence across the channel at a flow velocity of 7.5 mm/s.

The intensity of the fluorescence signal as a function of distance across the channel was plotted as a line profile. Figure 3(d) shows intensity line profiles for both positions 1 and 2 measured at 0.075, 1.5, and 15 mm/s, data for the other flow speeds not shown. The line profiles clearly show large linear regions in the center of the channel spanning over a distance of approximately 250 μm. In close proximity to the channel walls (within circa 50 μm), the profile differed slightly for the different flow rates and was attributed to the lower flow velocity in this near-wall region.[21] Fiber mats positioned in the center of the channel will be located within the linear portion of the gradient.

The differences in gradient profiles between positions 1 and 2 were expected from the simulation results and are due to diffusive mixing. At high flow velocities and short distances from the inlet, a stepwise profile can be seen which originates from the discrete concentration steps of the gradient network that are not overcome by diffusion. It can also be seen that the profiles for different flow velocities do not have a single intersection point in the middle of the channel,

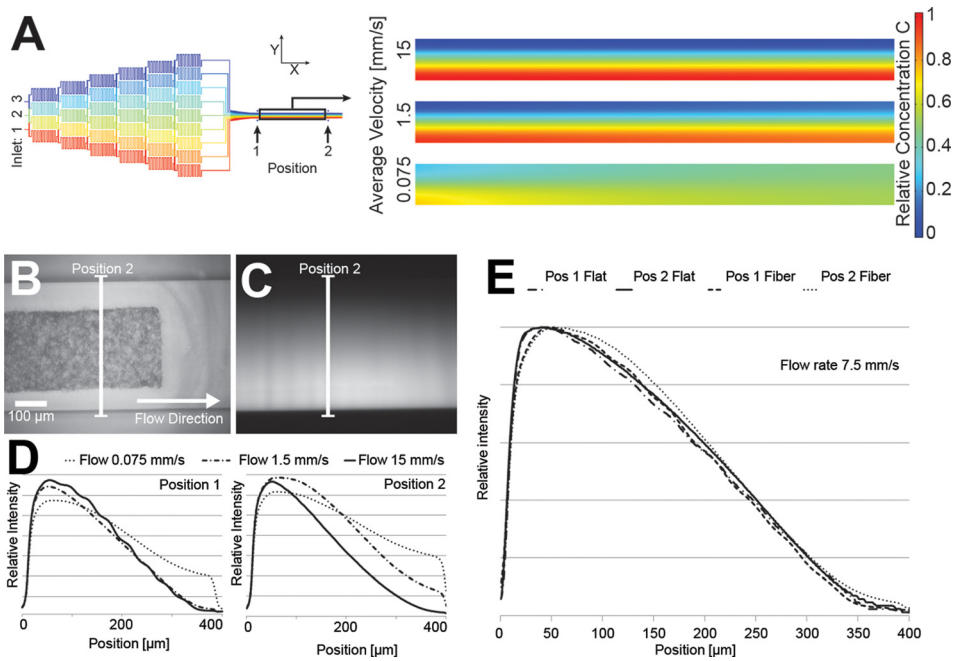

FIG. 3. (a) Simulated color coded concentration gradients in the microfluidic network (x-y plane). Left side: overview of the gradient network and downstream probing channel. The two measurement positions 1 and 2 are indicated. Right side: Magnification of the concentration gradient within the probing channel simulated for flow velocities of 0.075, 1.5, and 15 mm/s. (b) Bright field micrograph of an electrospun fiber pad in the microfluidic probing channel. The position for the intensity line profile measurement (position 2) is indicated in the figure, as well as the direction of flow. (c) Fluorescence micrograph of soluble sodium fluorescein gradient; the image was taken at the same position as indicated in (b) at a flow velocity of 7.5 mm/s. (d) Fluorescence intensity line profiles measured in microfluidic channels with fiber pads. The profiles were taken at the two different positions indicated in (a). Intensity line profiles are shown for flow velocities of 0.075, 1.5, and 15 mm/s. (e) Comparison of intensity line profiles in channels with (fiber) and without fiber pads (flat) measured at positions 1 and 2. These measurements were all done at a flow velocity of 7.5 mm/s.

as expected from the simulations. There are several possible reasons why this is not observed in the experimental setup. The measurements were performed by successively stepwise decreasing the flow velocity. This approach might lead to the problem that the probing channel is not completely cleaned and the flow profile not fully developed, at the time of analysis. Additionally, organic dyes, like sodium fluorescein, show a tendency to self-quench at higher concentrations, thus the relation between concentration and intensity shows non-linearity effects that could affect the measurements.[74] Even though, the features of the SU-8 master were measured, a small discrepancy between the computer model dimensions and the elastic PDMS channels could contribute to the minor differences between simulation and experimental data.

In general, the results of the gradient evaluation are in good accordance with the previous published results from other groups working with flat glass surfaces, similar gradient generator networks, and using fluorescence probes to determine gradient properites.[29,75] Differences are mainly attributed to variations in channel dimensions and flow rates used in the studies. Regardless of these variations, the overall linearity and shape of the gradient in our system are similar to that reported earlier.

Our primary interest, both in the simulation, as well as in the experimental evaluation, was to explore the effect of the fiber pads on the flow properties and gradients generated in the channel. In order to evaluate the influence of the fibers on solution gradients generated experimentally, channels with and without fiber pads were compared at different flow rates of sodium fluorescein, and fluorescent intensity line profiles were taken at positions 1 and 2, as before. Figure 3(e) shows a comparison of gradient profiles in two different channels at both positions for a flow velocity of 7.5 mm/s. The line profiles are very similar and no systematic differences could be observed for any of the different flow velocities. There are slight differences at the

left wall (25–50 μm) between the flat sample and the fiber sample visible. This is most likely due to minor variations of the microfluidic channels, since two separate channels were needed for these measurements. These variations could come from slight deformation during molding or bonding in the production process. In general, the results indicate that fiber mats with an approximated height of 5 μm do not significantly influence gradient formation, steepness, or bulk flow properties, thereby implying the applicability of patterned electrospun fibers in combination with complex microfluidic functionalities such as gradient generators.

A limiting factor of these experiments is that fluorescence intensity was measured in the whole fluid volume. Therefore, it is difficult to evaluate experimentally the exact flow properties on or near the fiber surface. In order to evaluate the interface properties between the liquid and the fiber pad in more detail, a second CFD simulation model was used. Figure 4(a) shows the simulated velocity magnitude (color coded blue = slow, red = fast) in the x-z cross section at the edge of the fiber pad for an average inflow velocity of 1.5 mm/s. There is nearly no flow within the fiber pad and the fiber pad is reducing the effective height of the channel from 50 μm to 45 μm for the free media flow. Thus, the maximum velocity in the center of the channel is higher (dark red area in the center) above the fibers, because the same amount of liquid has to pass through an effectively narrower channel in the same time. This is an expected effect and does not pose any problems for the current application when 5 μm thick fiber pads are used, but is very important to consider for thicker constructs, since free media flow gets more and more restricted. Figure 5(a) shows line profiles of relative concentration for an increasing simulated thickness. The relative concentration was always measured 2 μm above the fibers to investigate the gradient properties at the interface where the cells are. The data show that gradient steepness decreases with increasing fiber pad thickness due to a reduction of effective height for free media flow. This effect is further illustrated in Figures 5(b) and 5(c), showing cross-sections of color coded relative intensity and stream line profiles for 5, 20, and 40 μm thick fiber patterns, respectively. As the pad becomes thicker the flow gets more restricted and thus there is nearly no gradient for 40 μm. However, a height of 5 μm, as used in this study, does not significantly influence the gradient for the cells.

Figure 4(b) shows the vorticity magnitude (color coded blue = low, red = high) magnified at the edge of the fiber pad. The vorticity magnitude is a measure of the rotation in a fluid and is calculated as the curl of the fluid velocity vector. There is a small eddy forming at the edge

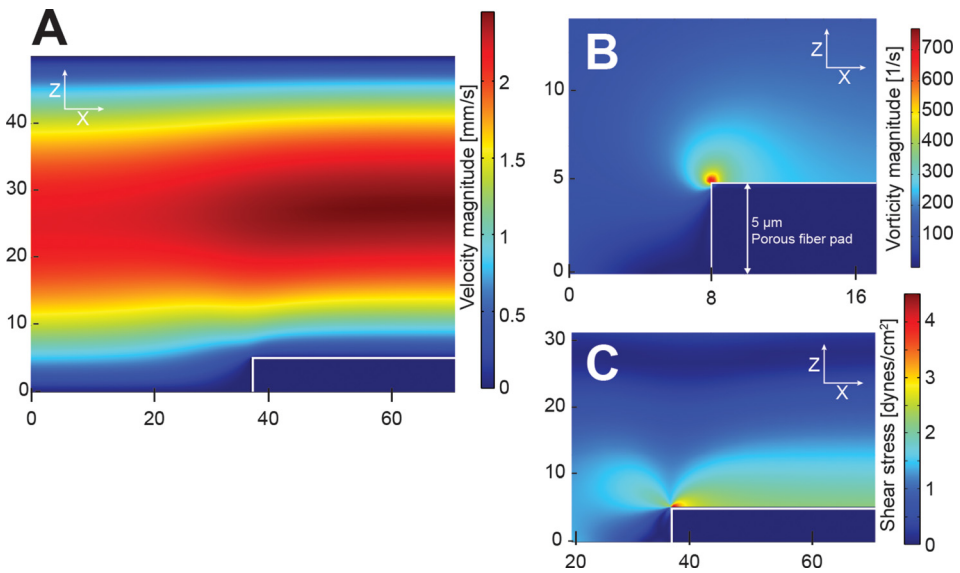

FIG. 4. (a) Simulated flow velocity profile in the probing channel, fiber pad indicated with a white line, for an average inflow velocity of 1.5 mm/s (x-z plane coordinates given in μm). (b) Simulated shear stress in the bottom half of the probing channel with similar simulation parameters as A. (c) Simulated vorticity magnitude at the edge of the fiber pad with similar simulation parameters as A and B.

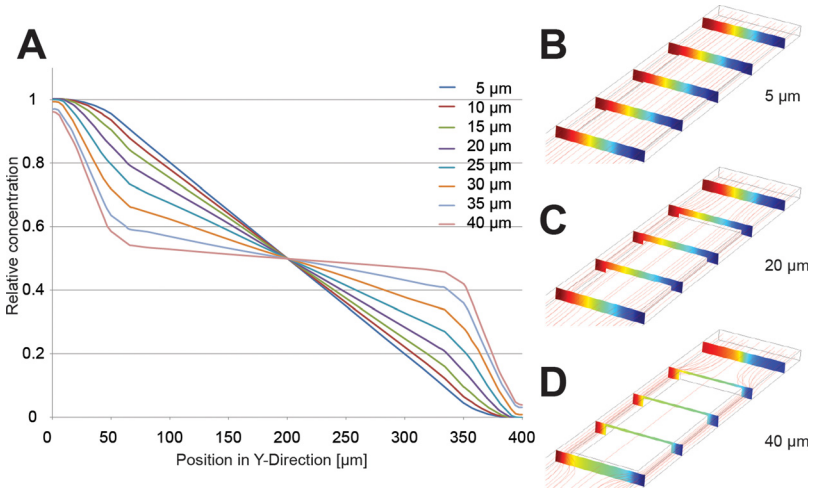

FIG. 5. (a) Simulated relative concentration line profiles for different fiber mat thicknesses for an average inflow velocity of 1.5 mm/s. The line profiles were taken 2 μm above each simulated fiber mat. (b), (c) and (d) Color coded relative concentration (red = high, blue = low) shown as cross-sections in the z-y plane and flow streamlines shown in red along the channel for 5, 20, and 40 μm thick fiber mats.

of the pad which is only locally extending into the free media flow, 5 μm in the z-direction and 10 μm in the x-direction. For cell experiments, such a disruption should be unproblematic, since the cells are located at the top surface and the local edge effect of several micrometers is much smaller than the cell size (laterally several tens of micrometers). It is, though, possible that the small disruptions result in changed concentrations and fluid exchange properties directly at the interface. However, the effect of local disturbance is over estimated in the simulation due to the fact that the fibers do not exhibit a sharp edge in reality. It is difficult to model such a edge in more detail since the actual topographies vary slightly from batch to batch.

In general, the simulation shows that laminar flow properties are retained in the main part of the channel, which supports the experimental data that liquid gradient formation is not disturbed by the fibers.

Cell culture on electrospun fibers in a microfluidic channel

The possibility to use the developed microfluidic system for maintaining cells in culture was studied using 3T3 fibroblasts. After a 2 h attachment period under static conditions, the cells were exposed to continuous flow of 1.5 mm/s. This corresponds to a volumetric flow rate of 30 nl/s, meaning that the total liquid volume of the probing channel (400 nl) is exchanged in less than 15 s. CFD simulations were performed to investigate the resulting shear stress in more detail using following equation:

$$\tau - \mu\left(\frac{du}{dz} + \frac{dw}{dx}\right). \tag{1}$$

The shear stress tensor (τ) can be approximated as the sum of the derivative of the flow velocity u with respect to position z and the derivative of the flow velocity w with respect to position x, multiplied by the dynamic viscosity, μ. The solution of Eq. (1), as calculated in COMSOL, results in the shear stress distribution shown in Figure 4(c). The figure shows the bottom half of the microfluidic channel including the edge of the fiber pad. The maximum shear stress is observed directly at the front edge of the fiber pad and is below 5 dyn/cm^2. On the remaining fiber pad, the shear stress is between 2 and 2.3 dyn/cm^2 at the interface between the fibers and the fluid. Cellular response upon shear stress varies widely depending on the cell type, but the amount of shear stress simulated for this setup is way below values associated with, e.g., fibroblast detachment, which are above 100 dyn/cm^2 for cell culture substrates.[76,77]

Figure 6 shows 3T3 fibroblast cells cultured in the microfluidic channel after 24 h under continuous flow of 1.5 mm/s. In the false colored composite fluorescent micrograph (Figure 6(a)), it can be seen that cells are attaching both to the randomly orientated fibers as well as to the surrounding glass substrate. Cell morphology and actin filament organization (red channel Figure 6(b)) were found to be similar to cells cultured on electrospun fibers or glass substrates in traditional Petri dishes without microfluidic networks (data not shown). Figures 6(b)–6(d) show separately the actin filaments in the red channel, the autofluorescence of the fibers in the green channel and the cell nuclei in the blue channel, respectively. Figures 6(e) and 6(f) show two other fiber pads along the length of the probing channel with cells attached to fibers. A more detailed image of a single cell attached and spread on an electrospun fiber mat is shown in Figure 6(g). The cell is clearly interacting with the fibers and it can be seen that the actin filaments are partially aligned to the underlying fiber substrate. Thus, we have found that it is possible to culture and maintain cells within the microfluidic channels, and that those cells can attach and spread on the electrospun fibers as they do if cultured outside of the channels.

One important aspect for the application of the proposed system for cell culture is the injection of cells into the microfluidic network. The cell seeding procedure was optimized to maximize cell survival and minimize problems like cell aggregation in the microfluidic network. It was found beneficial to inject the cells via the outlet port to avoid clogging in the long and fairly small channels of the gradient generator network. Furthermore, it was very important to let the cells adhere adequately to the substrate before exposing them to continuous flow. The cells were not able to settle and form a sufficient attachment on the surface under continuous flow. An attachment time of 2 h was proven to be sufficient for our experiments, which is in good agreement with attachment times reported in the literature.[78]

Neural stem cells were used to show the suitability of the platform to stimulate cells and study their response to chemical gradients in combination with aligned electrospun fibers. Figures 7(a) and 7(b) show clusters of neural stem cells, i.e., neurospheres, seeded on PORN/

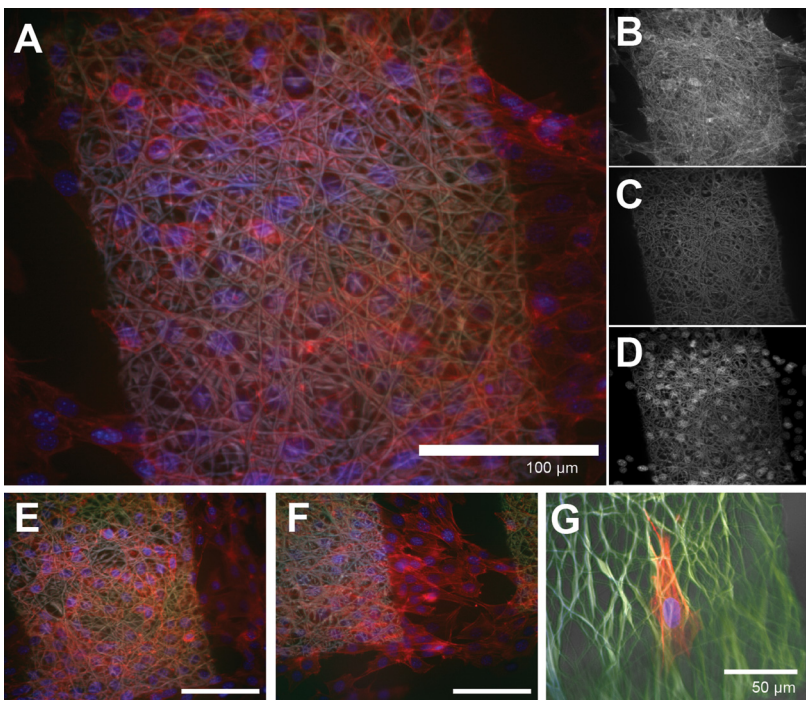

FIG. 6. (a) False color fluorescence micrograph of 3T3 fibroblast cells after 24 h of culture in the microfluidic network on electrospun fibers. Individual fluorescence channels shown in (b)-(d). (b) Red = actin filaments stained with Alexa Fluor555 phalloidin, (c) Green = autofluorescence of the fibers and (d) Blue = DNA stained with DAPI. (e) and (f) False colored fluorescence micrographs of cells situated in the microfluidic channel at different positions along the length of the probing channel (g) False colored fluorescence micrograph of a single cell on a fiber pad. All same color scheme as A.

laminin coated aligned electrospun fibers and a PORN/laminin coated glass surface, respectively. Cells are stained for glial fibrillary acidic protein (GFAP) in green which is an astrocyte marker and the cell nuclei are stained with DAPI in blue. These samples were cultured under static conditions in Petri dishes and were used as controls to verify that cells are aligning along fibers. This can be seen in Figure 7(a), where cells are preferentially growing out from the sphere along the fibers, whereas cells on a flat surface (Figure 7(b)) do not show this behavior and outgrowth is randomly orientated. Cell alignment along orientated electrospun fibers has been shown previously for different cell types,[79,80] and Lim *et.al* observed similar behavior as we do for adult neural stem cells.[81] An interesting observation in comparing Figures 7(a) and 7(b) is the GFAP-

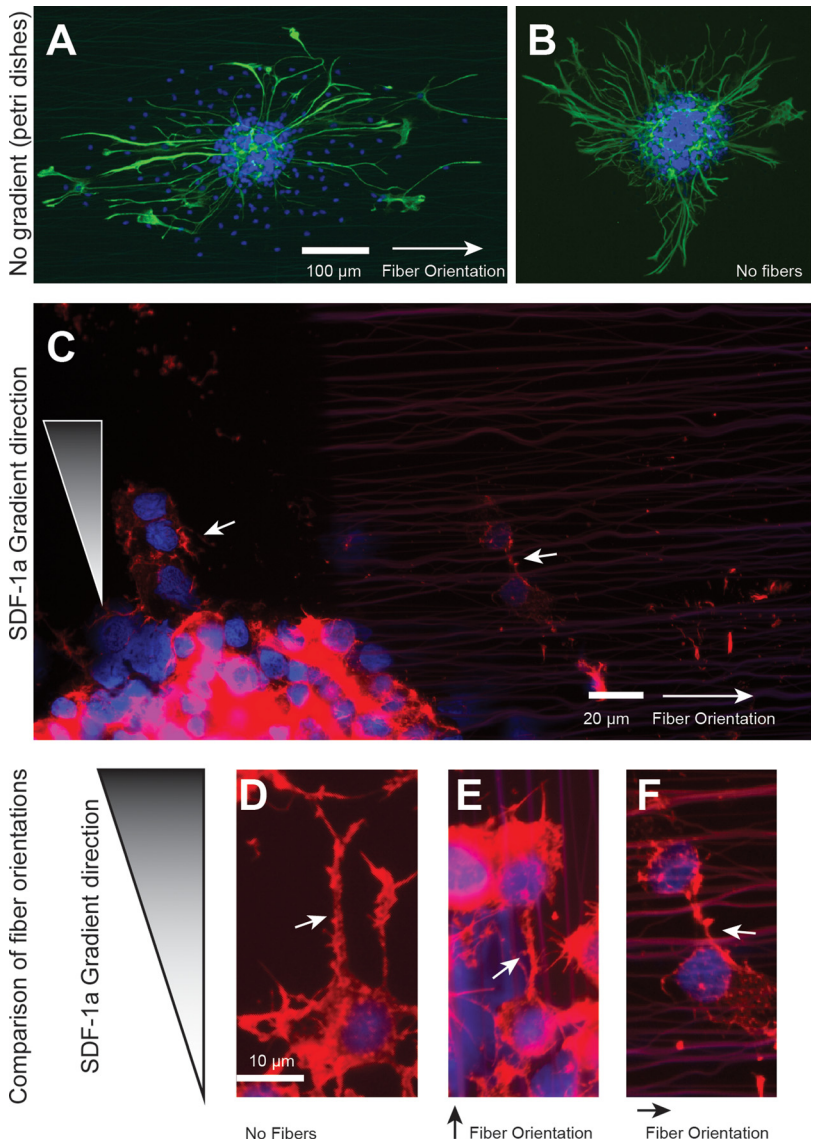

FIG. 7. (a) False color fluorescence micrograph of a neurosphere on laminin coated aligned electrospun fibers after 24 h of culture in a Petri dish. Green = GFAP and Blue = DNA stained with DAPI. (b) False color fluorescence micrograph of a neurosphere cultured on similar conditions than (a), but on a laminin coated flat glass surface. (c) False color fluorescence micrograph of neural stem cells in a microfluidic channel with a SDF-1a gradient increasing concentration from the bottom to top of the figure (as indicated by the wedge) partly on aligned electrospun fibers on the right side of the image(all surfaces coated with laminin) after 24 h of culture. Red = Actin filaments stained with Alexa Fluor555 phalloidin and Blue = DNA stained with DAPI. D-F) False color fluorescence micrograph of neural stem cells in a microfluidic chip cultured under similar conditions as (c) showing the three different conditions: without fibers (d), fibers orientated in parallel to the gradient (e) and fibers orientated perpendicular to the gradient (f).

negative cell migration, seen by DAPI staining, out from the neurosphere for spheres on electrospun fiber substrates. The underlying mechanism is currently under investigation.

The ability to inject whole neurospheres, with a diameter of approximately 100 μm, into the small microfluidic channels is limited and therefore, single cell solutions of disassociated neurospheres or very small spheres were used in the microfluidic experiments. Figure 7(c) shows cells in a microfluidic chip with patterned aligned electrospun fibers, where a gradient was applied, high concentration of SDF-1a at the top and low concentration at the bottom. Instead of GFAP, the actin cytoskeleton was stained in red and again cell nuclei in blue. Cells both on fibers, as well as on the glass between fiber pads, respond to the chemical SDF-1a gradient and a directional outgrowth up the gradient is visible.

The potential of the developed system to study the interplay between spatially and geometrically, well-controlled, electrospun patterns and gradients of soluble cues is demonstrated in Figures 7(d)–7(f) which shows micrographs of the three different combinations of fiber orientation and SDF-1a gradient conditions. Figure 7(d) is the control condition showing that cells on a flat surface are responding to the chemical gradient, as the cell philapodia are aligned in the direction up the gradient. Figure 7(e) is the condition with fibers aligned parallel to the gradient and thereby having both stimuli acting in the same direction, and Figure 7(f) is the condition with fibers aligned perpendicular to the gradient which means that the two cues are acting in orthogonal directions. The images show that cells are responding stronger to the chemical stimulus than the topographical, because in Figure 7(f) cell outgrowth is along the gradient, but perpendicular to the fibers.

This experiment illustrates the potential of the developed system and its ability to look at defined complex microenvironments composed of multiple cues in a systematic manner. A more thorough study is, however, needed to elucidate the interaction between contact guidance cues and chemical gradients on the outgrowth behavior of neural stem cells. The methodology and resulting microfluidic system presented here open the possibility for numerous investigations on the behavior of cells in well-defined microenvironments.

CONCLUSIONS

In this study, a new method to integrate patterned electrospun fiber pads with microfluidic networks was developed and successfully demonstrated. The approach is straightforward and does not influence nor imply any restrictions for the microfluidic network design, thus enabling highly controllable and flexible systems to generate multi parametric microenvironments for cell culture. It was shown that small patterned fiber pads with defined fiber alignment can be produced and that several fiber pads with varying fiber orientation can be deposited and patterned on one single substrate in subsequent steps. Computational fluid dynamics simulations as well as experimentally determined linear concentration gradients showed that the fiber pads do not significantly disturb the laminar flow in the microfluidic channel. It was shown that cells can be cultured in the system under mild flow conditions for at least 24 h, and that cells can be visualized *in situ* by bright field and fluorescent microscopies.

The full potential of the system to study the combined effects of surface topography and chemical gradients was demonstrated by culture of neural stem cells in microfluidic channels on aligned electro spun fibers. This preliminary data show the ability to study cell outgrowth in response to a chemical gradient under three main substrate configurations: a flat surface, aligned fibers parallel to the gradient, and aligned fibers perpendicular to the surface.

The system developed and demonstrated offers a large potential for the formation and control of cell microenvironments *in vitro* by offering spatially defined fibrous structures in combination with accurate control of the liquid environment.

ACKNOWLEDGMENTS

The research leading to these results has received funding from the European Union Seventh Framework Programme (FP7/2007-2013) under Grant Agreement Nos. NMP4-LA-2009-229289

NanoII and NMP3-SL-2009-229294 NanoCARD, from Vinnova under Contract No. 2009-00227 "Scaffolding nanomaterials for stem cell proliferation, migration and neural differentiation" and was carried out within the Sustainable Production Initiative and the Production Area of Advance at Chalmers.

[1]E. W. K. Young and D. J. Beebe, Chem. Soc. Rev. **39**, 1036–1048 (2010).
[2]J. Becerra, L. Santos-Ruiz, J. A. Andrades, and M. Marí-Beffa, Stem Cell Rev. **7**, 248–255 (2011).
[3]D. E. Discher, D. J. Mooney, and P. W. Zandstra, Science **324**, 1673–1677 (2009).
[4]J. a Burdick and G. Vunjak-Novakovic, Tissue Eng. Part A **15**, 205–219 (2009).
[5]I. K. Zervantonakis, C. R. Kothapalli, S. Chung, R. Sudo, and R. D. Kamm, Biomicrofluidics **5**, 13406 (2011).
[6]T. Vazin and D. V. Schaffer, Trends Biotechnol. **28**, 117–124 (2010).
[7]D. C. Dorn and A. Dorn, Stem Cell Res. **6**, 112–128 (2011).
[8]S. Krause, M. V. Maffini, A. M. Soto, and C. Sonnenschein, BMC Cancer **10**, 263 (2010).
[9]D. Wlodkowic and J. M. Cooper, Curr. Opin. Chem. Biol. **14**, 556–567 (2010).
[10]J. Liu, Y. Zhang, J. Zhao, Z. Yang, D. Li, F. Katirai, and B. Huang, Cancer Metastasis Rev. **30**, 177–184 (2011).
[11]N. A. Raof, W. K. Raja, J. Castracane, and Y. Xie, Biomaterials **32**, 4130–4139 (2011).
[12]N. T. Elliott and F. Yuan, J. Pharm. Sci. **100**, 59–74 (2011).
[13]Y. Lai, A. Asthana, and W. S. Kisaalita, Drug Discovery Today **16**, 293–297 (2011).
[14]A. Sica, C. Porta, E. Riboldi, and M. Locati, Eur. J. Immunol. **8**, 2131–2133 (2010).
[15]L. Sujata and S. Chaudhuri, Cell. Mol. Immunol. **5**, 107–112 (2008).
[16]D. Huh, G. a. Hamilton, and D. E. Ingber, Trends Cell Biol. **21**, 745–754 (2011).
[17]S.-J. Wang, W. Saadi, F. Lin, C. Minh-Canh Nguyen, and N. Li Jeon, Exp. Cell Res. **300**, 180–189 (2004).
[18]G. M. Whitesides, Nature **442**, 368–373 (2006).
[19]D. Mark, S. Haeberle, G. Roth, F. von Stetten, and R. Zengerle, Chemical Soc. Rev. **39**, 1153–1182 (2010).
[20]S. Kim, H. J. Kim, and N. L. Jeon, Integr. Biol. **2**, 584–603 (2010).
[21]T. Squires and S. Quake, Rev. Mod. Phys. **77**, 977–1026 (2005).
[22]E. Dahan, V. Bize, T. Lehnert, J.-D. Horisberger, and M. A. M. Gijs, Lab Chip **8**, 1809–1818 (2008).
[23]C.-Y. Chen, A. M. Wo, and D.-S. Jong, Lab Chip **12**, 794–801 (2012).
[24]C. S. Goodman, Annu. Rev. Neurosci. **19**, 341–77 (1996).
[25]J. B. Gurdon and P. Y. Bourillot, Nature **413**, 797–803 (2001).
[26]T. Bogenrieder and M. Herlyn, Oncogene **22**, 6524–6536 (2003).
[27]N. Ye, J. Qin, W. Shi, X. Liu, and B. Lin, Lab Chip **7**, 1696–1704 (2007).
[28]N. L. Jeon, S. K. W. Dertinger, D. T. Chiu, I. S. Choi, A. D. Stroock, and G. M. Whitesides, Langmuir **16**, 8311–8316 (2000).
[29]S. K. W. Dertinger, D. T. Chiu, N. L. Jeon, and G. M. Whitesides, Anal. Chem. **73**, 1240–1246 (2001).
[30]F. Lin, W. Saadi, S. W. Rhee, S.-J. Wang, S. Mittal, and N. L. Jeon, Lab Chip **4**, 164–167 (2004).
[31]D. Li and Y. Xia, Adv. Mater. **16**, 1151–1170 (2004).
[32]K. Garg and G. L. Bowlin, Biomicrofluidics **5**, 13403 (2011).
[33]C. J. Buchko, L. C. Chen, Y. Shen, and D. C. Martin, Polymer **40**, 7397–7407 (1999).
[34]G. L. Bowlin, K. J. Pawlowski, J. D. Stitzel, E. D. Boland, D. G. Simpson, J. B. Fenn, and G. E. Wnek, in *Tissue Engineering and Biodegradable Equivalents: Scientific and Clinical Applications*, edited by K. Lewandrowsky, D. J. Trantolo, J. D. Gresser, M. J. Yaszemski, D. E. Altobelli, and D. L. Wise (Marcel Dekker Inc., New York, 2002), pp. 165–178.
[35]W.-J. Li, C. T. Laurencin, E. J. Caterson, R. S. Tuan, and F. K. Ko, J.Biomed. Mater. Res. **60**, 613–621 (2002).
[36]J. A. Matthews, G. E. Wnek, D. G. Simpson, and G. L. Bowlin, Biomacromolecules **3**, 232–238 (2002).
[37]D. W. Hutmacher and P. D. Dalton, Chem. Asian J. **6**, 44–56 (2011).
[38]Q. P. Pham, U. Sharma, and A. G. Mikos, Biomacromolecules **7**, 2796–2805 (2006).
[39]A. K. Ekaputra, G. D. Prestwich, S. M. Cool, and D. W. Hutmacher, Biomacromolecules **9**, 2097–2103 (2008).
[40]B.-M. Min, G. Lee, S. H. Kim, Y. S. Nam, T. S. Lee, and W. H. Park, Biomaterials **25**, 1289–1297 (2004).
[41]M. Chen, P. K. Patra, M. L. Lovett, D. L. Kaplan, and S. Bhowmick, J. Tissue Eng. Regener. Med. **3**, 269–279 (2009).
[42]C. A. Bashur, R. D. Shaffer, L. A. Dahlgren, S. A. Guelcher, and A. S. Goldstein, Tissue Eng. Part A **15**, 2435–2445 (2009).
[43]B. Carlberg, M. Z. Axell, U. Nannmark, J. Liu, and H. G. Kuhn, Biomed. Mater. **4**, 045004 (2009).
[44]G. T. Christopherson, H. Song, and H.-Q. Mao, Biomaterials **30**, 556–564 (2009).
[45]B. M. Whited, J. R. Whitney, M. C. Hofmann, Y. Xu, and M. N. Rylander, Biomaterials **32**, 2294–2304 (2010).
[46]E. Schnell, K. Klinkhammer, S. Balzer, G. Brook, D. Klee, P. Dalton, and J. Mey, Biomaterials **28**, 3012–3025 (2007).
[47]H. B. Wang, M. E. Mullins, J. M. Cregg, C. W. McCarthy, and R. J. Gilbert, Acta Biomater. **6**, 2970–2978 (2010).
[48]B. Carlberg, T. Wang, and J. Liu, Langmuir **26**, 2235–2239 (2010).
[49]J. Imitola, K. Raddassi, K. I. Park, F.-J. Mueller, M. Nieto, Y. D. Teng, D. Frenkel, J. Li, R. L. Sidman, C. A. Walsh, E. Y. Snyder, and S. J. Khoury, Proc. Natl. Acad. Sci. U.S.A. **101**, 18117–18122 (2004).
[50]P. Roach, T. Parker, N. Gadegaard, and M. R. Alexander, Surf. Sci. Rep. **65**, 145–173 (2010).
[51]G. Fishell and A. R. Kriegstein, Curr. Opin. Neurobiol. **13**, 34–41 (2003).
[52]J. C. McDonald, D. C. Duffy, J. R. Anderson, D. T. Chiu, H. Wu, O. J. Schueller, and G. M. Whitesides, Electrophoresis **21**, 27–40 (2000).
[53]B. M. Fu, F. E. Curry, and S. Weinbaum, Am. J. Physiol. **269**, H21247–H2140 (1995).
[54]L. Durlofsky and J. F. Brady, Phys. Fluids **30**, 3329 (1987).
[55]L. Moscou and S. Lub, Powder Technol. **29**, 45–52 (1981).
[56]J. G. Berryman and S. C. Blair, J. Appl. Phys. **60**, 1930 (1986).
[57]S. M. Kim, S. H. Lee, and K. Y. Suh, Lab Chip **8**, 1015–1023 (2008).
[58]C.-H. Hsu and A. Folch, Appl. Phys. Lett. **86**, 023508 (2005).

[59]N. Li and A. Folch, Exp. Cell Res. **311**, 307–16 (2005).
[60]See supplementary material at http://dx.doi.org/10.1063/1.4729747 for Fig. X1 (additional Patterns of Fiber Pads) and Fig. X2 (cross-section of a Misaligned Microfluidic Channel Where the Fiber Pad Is Disturbing the Seal).
[61]T. D. Brown, P. D. Dalton, and D. W. Hutmacher, Adv. Mater. **23**, 5651–5657 (2011).
[62]J. Kameoka, R. Orth, Y. Yang, D. Czaplewski, R. Mathers, G. W. Coates, and H. G. Craighead, Nanotechnology **14**, 1124–1129 (2003).
[63]C. Chang, K. Limkrailassiri, and L. Lin, Appl. Phys. Lett. **93**, 123111 (2008).
[64]T. D. Brown, P. D. Dalton, and D. W. Hutmacher, Adv. Mater. **23**, 5651–5657 (2011).
[65]D. Sun, C. Chang, S. Li, and L. Lin, Nano Lett. **6**, 839–842 (2006).
[66]W. Y. Yeong, H. Yu, K. P. Lim, K. L. G. Ng, Y. C. F. Boey, V. S. Subbu, and L. P. Tan, Tissue Eng. Part C **16**, 1011–1021 2010).
[67]R. Chang, K. Emami, H. Wu, and W. Sun, Biofabrication **2**, 045004 (2010).
[68]N. L. Nerurkar, S. Sen, B. M. Baker, D. M. Elliott, and R. L. Mauck, Acta Biomater. **7**, 485–491 (2011).
[69]L. Kim, Y.-C. Toh, J. Voldman, and H. Yu, Lab Chip **7**, 681–694 (2007).
[70]S. Bhattacharya, A. Datta, J. M. Berg, and S. Gangopadhyay, J. Microelectromech. Syst. **14**, 590–597 (2005).
[71]D. Yang, X. Niu, Y. Liu, Y. Wang, X. Gu, L. Song, R. Zhao, L. Ma, Y. Shao, and X. Jiang, Adv. Mater. **20**, 4770–4775 (2008).
[72]E. Jo, M.-C. Lim, H.-N. Kim, H.-J. Paik, Y.-R. Kim, and U. Jeong, J. Polym. Sci., Part B: Polym. Phys. **49**, 89–95 (2011).
[73]Y. Liu, D. Yang, T. Yu, and X. Jiang, Electrophoresis **30**, 3269–3275 (2009).
[74]P. Bojarski, L. Kulak, C. Bojarski, and A. Kawski, J. Fluoresc. **5**, 307–319 (1995).
[75]K. Campbell and A. Groisman, Lab Chip **7**, 264–272 (2007).
[76]H. Lu, L. Y. Koo, W. M. Wang, D. A. Lauffenburger, L. G. Griffith, and K. F. Jensen, Anal. Chem. **76**, 5257–5264 (2004).
[77]C. Christophis, M. Grunze, and A. Rosenhahn, Phys. Chem. Chem. Phys. **12**, 4498–4504 (2010).
[78]G. A. Truskey and T. L. Proulx, Biomaterials **14**, 243–254 (1993).
[79]J. Xie, M. R. MacEwan, A. G. Schwartz, and Y. Xia, Nanoscale **2**, 35–44 (2010).
[80]V. Beachley, E. Katsanevakis, N. Zhang, X. Wen, and N. Zhang, Adv. Polym. Sci. **246/2012**, 171–212 (2012).
[81]S. H. Lim, X. Y. Liu, H. Song, K. J. Yarema, and H.-Q. Mao, Biomaterials **31**, 9031–9039 (2010).